Blunt Slender Cones in Viscous Hypersonic Flow

C. C. HORSTMAN*
NASA Ames Research Center, Moffett Field, Calif.

An experimental investigation has been conducted to obtain surface measurements and flowfield properties about blunt slender cones and to study viscous-inviscid coupling in hypersonic flow. The measurements, obtained on a 3° half-angle cone in helium at Mach 40, included surface pressures and heat transfer, shock-wave shapes, and detailed shock-layer surveys at angles of attack of 0°, 3°, ±5°, and ±10°. At zero angle of attack, significant changes caused by boundary-layer entropy-layer coupling were observed in the inviscid flowfield structure. An approximate theoretical inviscid-viscous calculation using a mass balance procedure to determine boundary-layer-edge quantities gave reasonable agreement with the experimentally determined surface quantities and shock-wave shapes. However, for the calculation of the details of a flowfield a more complicated analysis would be required. A correlation of blunt cone heat transfer was obtained for a range of Reynolds numbers including merged layer, viscous interaction, and thin boundary-layer cone flow regimes. At angle of attack on the windward cone rays, the flowfield structure and surface pressure distribution suggested that inviscid equivalent cone techniques are sufficient. The heat-transfer results indicated that neither equivalent cone nor approximate two-dimensional techniques are sufficient to predict the data.

Nomenclature

C_∞ = proportionality constant in temperature viscosity law, $C = [\mu(T_w)/\mu(T_\infty)](T_\infty/T_w)$
C^* = $[\mu(T^*)/\mu(T_\infty)](T_\infty/T^*)$
C_D = cone nose drag coefficient (reference area based on nose diameter)
C_H = Stanton number, $q/\rho_\infty u_\infty C_p(T_{aw} - T_w)$
C_p = specific heat at constant pressure
D = cone nose diameter
M = Mach number
p = pressure
p_{t_2} = measured pitot pressure
q = local surface heating rate
R = cone nose radius
Re = Reynolds number
T = temperature
T^* = $T_o[1 + 3(T_w/T_o)]/6$
u = local stream velocity
x = distance along cone axis with the origin at the nose
y = radial distance from cone axis
α = angle of attack
γ = ratio of specific heats
Δ = distance from cone surface (perpendicular to cone axis)
ϵ = $\gamma - 1/\gamma + 1$
θ_c = cone semivertex angle
μ = viscosity
ρ = density

Subscripts

aw = adiabatic wall
o = stagnation
w = wall
s = value at shock wave
∞ = free stream
2 = value behind normal shock wave

I. Introduction

At low Reynolds numbers the complex nature of the hypersonic flow over blunt bodies is due to viscous-inviscid coupling. The interaction between the inviscid "entropy" layer (the fluid close to the body which has passed through the curved portion of the shock wave) and the boundary layer has been theoretically treated using a wide variety of approximations.[1-6] However, with the exception of the recent work by Little and Marchand,[4] detailed experimental information about the character of the flowfield is lacking in the regime where the viscous boundary layer comprises a considerable portion of the flowfield. For the most part, the comparisons between experiment and the various theories have only considered surface pressure, surface heat transfer, and/or total blunt-cone drag.[1,3] These comparisons have indicated unexplained differences resulting from the lack of a complete set of data, which includes flowfield surveys in addition to measured surface quantities.

The purpose of the present investigation was to obtain a complete set of measurements on blunt slender cones to determine the influence of the viscous boundary layer on the inviscid flowfield when the boundary layer is of the same order of thickness as the local body radius. These measurements, obtained on a 3° half angle cone at zero and small angles of attack (up to 10°), included surface pressure and heat transfer, shock-wave shapes, and flowfield surveys. Such an investigation can provide an insight into the details of the viscous-inviscid coupling mechanism and can be used to determine the applicability of present theoretical interaction solutions or perhaps provide a basis for a new theoretical approach consistent with experimental observations. Unfortunately, the recent analysis outlined by Cheng[6] applies to a more slender body than presently investigated. The viscous hypersonic "blunt-needle" problem remains unexplored experimentally.

II. Experimental Procedure

The test facility and experimental techniques used in the present investigation are essentially the same as those described in Ref. 7. A brief description of the facility, test models, and test techniques is presented below for completeness.

Mach 50 Helium Tunnel

This tunnel has a contoured nozzle with a 28-in.-diam nozzle exit and an open test section. The usable test core diameter is 6 in. The nominal stagnation conditions for the present series of tests using helium as a test gas were 1600 psia at 1500°R. A steam ejector system maintains a constant back pressure of less than 0.05 psia providing, for all practical purposes, a continuously running tunnel. The nominal test conditions were $M_\infty = 40$, and $Re_\infty/\text{in.} = 58{,}000$. For these

Received November 17, 1969; revision received April 2, 1970.
* Research Scientist. Member AIAA.

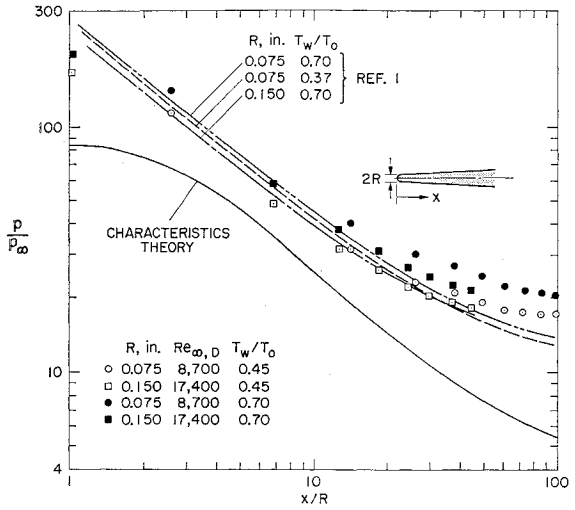

Fig. 1 Surface pressure distribution; $M_\infty = 40$, $\theta_c = 3°$, $\alpha = 0°$, $\gamma = \frac{5}{3}$.

conditions, the axial and transverse Mach number gradients were less than 0.1 and 0.3 in.$^{-1}$, respectively.

Test Model Configurations

The test models were 3° semivertex angle cones with hemispherical nose diameters of 0.15 and 0.30 in. Both configurations had a 1-in. base diameter. To determine the zero angle-of-attack location in the wind-tunnel test section, three pressure orifices were placed 120° apart near the base of each model used. The accuracy of the pitch and yaw angle was ±0.25°.

Surface Pressure Measurements

Surface pressures were measured on stainless steel models. The pressure orifices (varying in diameter from 0.047 to 0.117 in.) were located along a single cone ray from near the sphere-core junction to the model base. Stainless steel tubing connected each pressure orifice to pressure transducers at the base of the model support sting (a total length of 4 ft). Pressures were measured by Barocel variable capacitance transducers with full-scale ranges of 0–1000 μ Hg and 0–10,000 μHg. The measured pressures varied from 150-3000 μHg. Lag times encountered in the present series of tests varied from 10–25 sec.

The measured surface pressures were corrected for thermal transpiration effects in the orifice tube and the orifice effects due to heat transfer.[8] The magnitudes of these corrections were a maximum of 20% and 2%, respectively, for the test results. The experimental scatter in the corrected data was ±5%. The over-all accuracy of the wall pressure data reported was calculated to be within ±10%.

Heat-Transfer Measurements

Surface heat transfer was measured by the thin-walled transient technique. The models were constructed from hollow, electroformed, nickel shells with a 0.020-in.-thick wall. The thermocouple wires were inserted through 0.003-in.-diam holes in model surface and soldered in place. For a particular test, the model was preheated to the desired wall temperature and then inserted into the tunnel stream at the desired angle of attack. This insertion process took from 0.3 to 0.7 sec. The temperature-time history of each thermocuple was recorded on a multichannel high-speed data processor. The local heating rate vs wall temperature was plotted for a wide range of wall temperatures and the intersection of this curve and the zero heating rate axis was used for the local recovery temperature. The curvature of the model surface was taken into account in the evaluation of the effective skin thickness.[9] Use of the criteria developed in Refs. 10 and 11 shows that the errors due to tangential conduction in the thin wall and down the thermocouple wires were negligible for the present tests.

The most significant error in the heat-transfer measurements is the uncertainty of the recovery temperature because of the radiation corrections applied to the heating rate at high values of T_w/T_o. The experiment scatter in the data was ±7%. The over-all accuracy of the heat-transfer data presented was calculated to be within ±15%.

Glow Discharge Tests

Insulated brass models with a negative potential of about 300 v were used to determine shock wave shape. Photographs of the resulting glow discharge showed relative gas density as variations in light intensity. The measured shock-layer thicknesses indicated excellent agreement with pitot-pressure surveys obtained at discrete values of x/R.

Shock-Layer Surveys

Internally cooled, variable temperature models were used to investigate the flowfield over a blunt 3° semivertex cone with both a hot and a cold wall. Pitot pressure was measured with a rectangular stainless steel probe (the outside dimensions were 0.012-in. high by 0.035-in. wide with a uniform wall thickness of 0.0015 in.). The wind-tunnel test time and time response of the probe were such that a continuous sweep of the flowfield was possible. To determine rarefaction effects for the impact-probe measurements the probe was calibrated in a freejet facility.[12] For the present test conditions, the rarefaction effects are only significant close to the test model wall where the magnitude of the pitot pressure is small.

Total temperature was surveyed with a double shielded chromel-alumel total temperature probe 0.080-in. in diameter. Independent calibration of this probe in the freejet facility[12] indicated a maximum total temperature error of 10% for the present test conditions.

III. Results and Discussion

The experimental results obtained in the present investigation are presented in two sections. Zero angle-of-attack data are presented and compared with calculated results obtained from theory and with other published data in the first section. Angle-of-attack data are presented and compared with approximate theoretical techniques developed for cones at small angle of attack in the second section.

Zero Angle of Attack

The surface pressure data obtained for $T_w/T_o = 0.45$ and 0.70 are presented in Fig. 1. As the nose Reynolds number decreases and T_w/T_o increases, the pressure increases. This is consistent with previous viscous-inviscid interaction results, in that both a decreasing Reynolds number and an increasing T_w/T_o increase the boundary-layer thickness, thus increasing the effective test model thickness and surface pressure. The data show a substantial increase (up to 300%) in the surface pressure over the pressure predicted by inviscid characteristics theory.[13]

The present pressure distribution data are compared with computations based on Levine's analyses.[1] These computations combine through an iterative procedure a nonsimilar boundary-layer solution including transverse curvature with a characteristic's solution using a maws balance procedure to determine boundary-layer-edge properties. In each case the computation was started with an inviscid characteristics calculation. A boundary-layer solution is then obtained by assuming the pressure to be equal to the inviscid valve at the body surface. The other edge conditions are found by equating the boundary-layer mass flow at the point of interest to the

stream tube of equal mass in the freestream at the bow shock wave. Thus entropy and pressure at the boundary-layer edge are known from the inviscid solution and can be used to find edge enthalpy, temperature, and density. Since the edge conditions at a given location depend on the solution at that location, and vice versa, an iterative procedure is used. No attempt was made to match the normal gradients of the flow properties in the boundary-layer solution to the inviscid solution. The procedure was then repeated, replacing the model configuration in the inviscid characteristics calculation with an effective model shape (defined by adding the displacement thickness to the true model surface). Three complete iterations were performed for each of three test conditions ($M_\infty = 40, \gamma = 5/3; Re_{\infty,D} = 8700, T_w/T_o = 0.70$ and 0.37; and $Re_{\infty,D} = 17400, T_w/T_o = 0.70$). In each case, the iterations were converging (i.e., the results from the third iteration fell between the results from the first and second iterations.) The results predicted by the second and third iterations differed by about 20% except for the wall pressure results where the differences were slightly larger. Additional iterations would be required to obtain more accurate solutions.

The results of the computations compared with the present surface pressures (Fig. 1) agree well except for large x/R. With additional iterations the agreement between theory and experiment would improve at the larger values of x/R since the second and third iterations bracket the data. The computations also indicate an increasing pressure with decreasing nose Reynolds number and increasing T_w/T_o. However, the magnitude of the predicted pressure increases is less than experimentally observed.

Although data have been obtained for values of x/R up to 100, the entire range of x/R investigated is in the bluntness dominated cone flow regime so that a negative pressure gradient exists over the entire test model. Farther downstream the inviscid pressure will increase and approach the conic pressure. Therefore, care must be taken when the present results are compared to investigations[2-4] in which a significant portion of the data is downstream of the minimum pressure location where the cone nose no longer dominates the flowfield.

The surface heat-transfer data from the two test models at $T_w/T_o \approx 0.37$ are presented in Fig. 2. The data are presented in the form $C_H(Re_{\infty,D})^{1/2}$ vs x/R which is equivalent to local heat transfer normalized by the stagnation-point heat transfer $\sim (Re_{\infty,D})^{-1/2}$ vs x/R for a single freestream Mach number. The data correlate independently of nose Reynolds number. However, thin boundary-layer theory for blunt cones[14,15] predicts this type of correlation for a single pressure distribution and wall temperature and the measured pressure distributions for the two test models only differed by about 5% (Fig. 1).

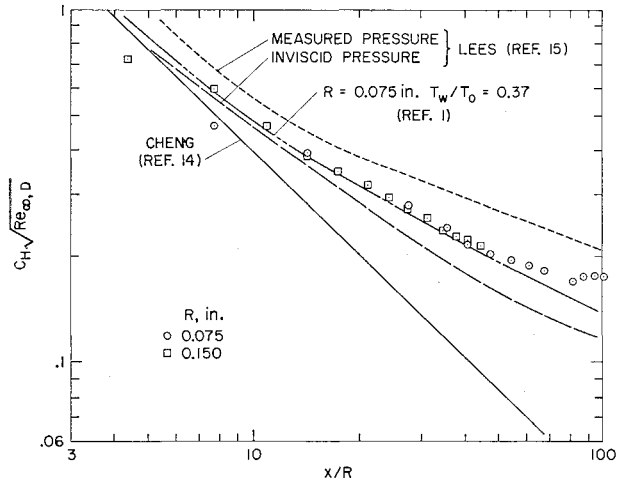

Fig. 2 Surface heat-transfer distribution; $M_\infty = 40$, $\theta_c = 3°$, $\alpha = 0°$, $T_w/T_o \approx 0.37$, $\gamma = \frac{5}{3}$.

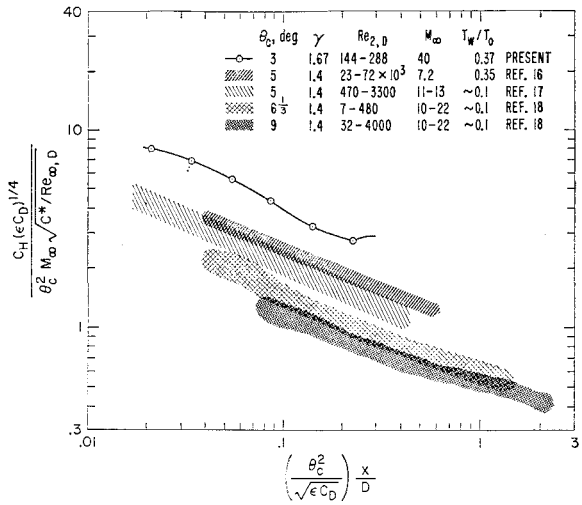

Fig. 3 Comparison with available heat-transfer data; $\alpha = 0°$.

The present heat-transfer data are compared with an inviscid-viscous computation,[1] Cheng's solution,[14] and Lees' blunt cone theory.[15] The measured pressure used in the Lee's calculation, was an average obtained for the two models at $T_w/T_o = 0.45$ (Fig. 1), and the inviscid pressure used was from characteristics theory (Fig. 1). The present data are in excellent agreement with the results of the inviscid-viscous computations.[1] Note that the Lees' prediction[15] using the measured pressure distribution substantially overpredicts the data. A correction to Lees' theory for transverse curvature effects[3] would further increase the disagreement with the experiment. It is evident from this comparison that the complete inviscid-viscous solution[1] is required to achieve adequate heat-transfer predictions in this type of flow regime.

Although they are not shown, limited data were obtained at elevated values of T_w/T_o to obtain recovery temperature. Within experimental accuracy ($\pm 15\%$), the Stanton number was found to be independent of T_w/T_o. The inviscid-viscous computation based on Ref. 1 also indicated that the Stanton number is invariant with T_w/T_o. The measured recovery ratios (T_{aw}/T_o) varied from 0.78 to 0.80.

The present heat-transfer data are compared with other available slender cone data (including recent data obtained in the Ames 3.5-Foot Hypersonic Wind Tunnel[16]) in Fig. 3, using Cheng's thin boundary-layer correlation coordinates[14] for a slender blunt cone. Cheng's coordinates were intended to account for variations in nose shapes, cone angle, freestream Mach number, and specific heat ratio, but they were not intended to account for transverse curvature, boundary-layer shock-wave interaction due to boundary-layer displacement effects, or boundary-layer shock-wave merging. The ordinate of this figure is proportional to the local heating rate normalized by the stagnation-point heating rate for a constant value of T_w/T_o, p_w/p_o, and γ[15]. For the present comparison, only data obtained in the bluntness dominated portion of the cone were included.

For a given cone angle, the data from widely differing flow regimes correlated in the sense that the ratio of local heat transfer to the continuum stagnation-point value for a given location on a cone is independent of Mach and Reynolds number. The fact that the data are cone angle dependent only indicates that Cheng's inviscid pressure distribution approximation is not valid for slender cones. The data included encompass merged, viscous-layer, and continuum nose flow regimes and strong-and-weak-interaction and thin boundary-layer cone-flow regimes. The fact that the heat-transfer ratios are independent of Mach and Reynolds numbers for a given cone angle is surprising since it has been previously noted that a complete inviscid-viscous solution was necessary

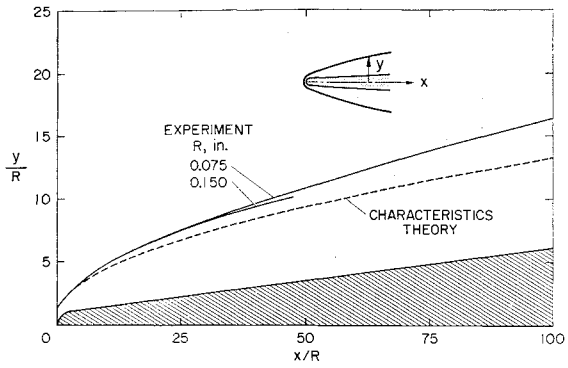

Fig. 4 Shock-wave shapes; $M_\infty = 40$, $\theta_c = 3°$, $\alpha = 0°$, $T_w/T_o \approx 0.70$, $\gamma = \frac{5}{3}$.

to predict the present results (Fig. 2). The implication is that this heat-transfer ratio is insensitive to boundary-layer shock-wave merging and second-order boundary-layer effects (transverse curvature and shock-wave displacement) in the cone-nose dominated portion of the flowfield. Theoretically, this unusual result could be verified by a series of complete inviscid-viscous blunt cone solutions over a large Reynolds number range. Previous sharp-cone data[7] obtained in the strong interaction flow regime were also found to be insensitive to transverse curvature and displacement effects.

Shock-wave shapes obtained from glow discharge photographs are shown in Fig. 4 for $T_w/T_o = 0.70$. Shock-wave shapes were also obtained at $T_w/T_o = 0.37$ and the results were similar to those shown in Fig. 4 with about a 3% reduction in total shock-layer thickness. The experimental results indicate a slight increase in shock-layer thickness and slope as the nose Reynolds number decreased. Also, the data show an increase in shock-layer thickness above the values predicted by characteristics theory.[13] This agrees qualitatively with the measured pressure results shown in Fig. 1(i.e., an increase in boundary-layer thickness caused by decreasing Reynolds number will increase both the pressure and shock-layer thickness). Although not shown in Fig. 4, the inviscid-viscous computations based on Ref. 1 agreed with the experimental shock-shape results (within 5%) for both test models.

Pitot pressure surveys through the shock layer obtained at various axial stations ($x/R = 10$, 30, and 80) are presented in Fig. 5 for $T_w/T_o = 0.70$. These results have not been corrected for rarefaction effects since these corrections are small compared to the scale of the figure [i.e., corrections for rarefaction effects are only significant, >5%, when $p_{t_2}/(p_{t_2})_\infty$ is less than 0.1]. As x/R increased from 10 to 80, the general character of the measured profiles gradually changes from inviscid to viscous. This is verified by the close agreement with inviscid characteristics solution at $x/R = 10$ and the similarity at $x/R = 80$ to a profile obtained for a sharp cone[7] at the same test conditions. Comparison of the measured results with the characteristics solution as a function of x/R indicate the increasing influence of the boundary layer as x/R increases. In fact, the shape of the measured profile indicates that the boundary layer and entropy layer have merged far downstream from the nose ($x/R = 80$). For the entire range of x/R investigated, the profiles are, for the most part, independent of nose Reynolds number, and, although not shown, profiles obtained at $T_w/T_o = 0.37$ were similar to the results at $T_w/T_o = 0.70$ except for a small region near the wall.

The computed results from the inviscid-viscous theory[1] are also compared with the experimental measurements for the model with nose radius equal to 0.075 in. It is seen that the agreement between theory and experiment is not as good as for the previously mentioned surface quantities. This is due to the computational procedure which makes no effort to match the boundary layer and inviscid layer at the boundary-layer edge. Since the viscous and inviscid solutions overlapped (the viscous boundary-layer solution was extended to the boundary-layer edge and the inviscid solution extended from the shock wave down to the edge of the boundary-layer displacement thickness), the boundary-layer results were arbitrarily faired into the inviscid results. The location of the faired portion of the solution can be seen in Fig. 5, where the theory crosses the data at the boundary-layer edge. The calculations for the larger nose radius and lower wall temperature were identical to the results indicated in Fig. 5, except in the vicinity of the boundary layer-inviscid layer boundary. In this region substantial differences were noted but could be attributed to the arbitrary fairing process used. A possible method for improving this fairing process would be the composite expansion method of Van Dyke.[4,19]

Velocity profiles can be calculated by combining the pitot-pressure and total-temperature measurements along with the assumption of constant static pressure through the boundary layer. The calculated velocity profiles are presented in Fig. 6 for $T_w/T_o = 0.7$ and $R = 0.075$ in. For the present calculations the static pressure was assumed equal to the wall pressure and the pitot-pressure measurements were corrected for rarefaction effects. The error limits superimposed on the velocity profile for $x/R = 50$ represent a combination of the uncertainty of the corrected pitot-pressure and total temperature measurements in addition to a ±50% variation in assumed static pressure. The calculated velocity profiles were essentially independent of nose Reynolds number, but they varied as a function of x/R. The results from the inviscid-viscous computations[1] are also shown in Fig. 6. In view of the lack of

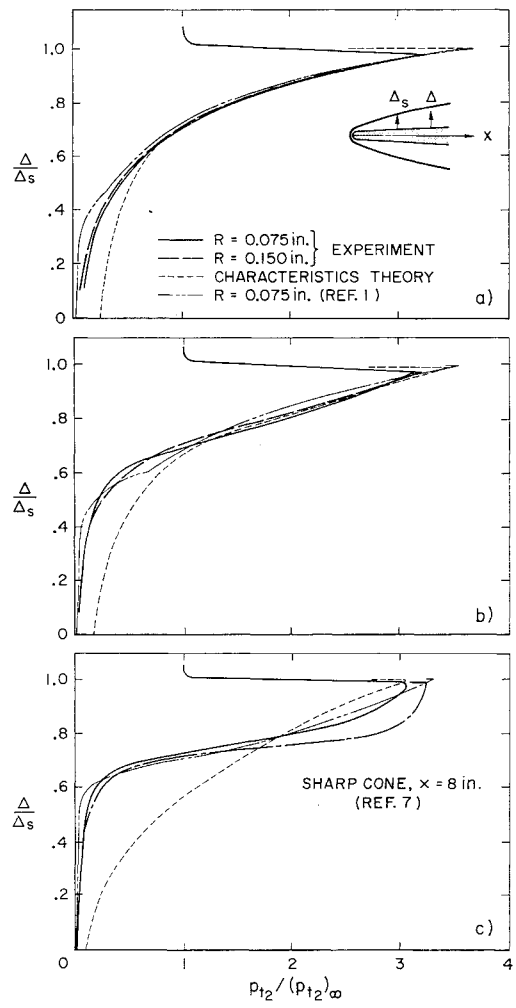

Fig. 5 Pitot-pressure profiles through the shock layer; $M_\infty = 40$, $\theta_c = 3°$, $\alpha = 0°$, $T_w/T_o \approx 0.70$, $\gamma = \frac{5}{3}$; a) $x/R = 10$, b) $x/R = 30$, c) $x/R = 80$.

a formal matching procedure at the outer edge of the boundary layer and the omission of normal static pressure gradients in the boundary-layer portion of the inviscid-viscous computations, the agreement between theory and experiment is reasonably good.

Angle of Attack

During the present investigation, surface pressure and heat-transfer data, pitot-pressure surveys, and shock-wave shapes were obtained at angles of attack equal to 1, 2, 3, 5, and 10° over the windward and leeward rays of the two blunt-cone configurations. The discussion here will be limited to the highlights of these results.

The surface pressure distribution on the windward and leeward cone rays are presented in Fig. 7 for $T_w/T_o = 0.7$. For comparison, the results of several inviscid equivalent cone characteristics solutions[13] are also shown. (The equivalent cone is a blunt cone whose cone half angle is equal to the angle of attack plus the cone half angle.) Except for $\alpha = 10°$, the surface pressure is slightly increased for the lower nose Reynolds number model indicating increased boundary-layer shock-wave interaction. At $\alpha = 5$ and 10°, the inviscid equivalent cone solution is in reasonable agreement with the experimental results for $x/R > 10$. However, the axial location of the pressure overexpansion is slightly downstream of the theoretically predicted location in each case. Possible explanations for this disagreement are an increased effective nose diameter due to a boundary-layer displacement thickness and/or the inaccuracy of the equivalent cone approximation itself. The data seem to indicate that for high angles of attack the flow over the windward rays of the cone is dominated by the inviscid flowfield as opposed to inviscid-viscous interactions. This has also been observed for sharp cones at angle of attack.[7]

It was shown previously that the blunt-cone heat transfer correlated independent of nose Reynolds number at zero angle of attack when plotted in the form $C_H\ (Re_{\infty,D})^{1/2}$ vs x/R. Therefore, the equivalent cone hypothesis at angle of attack could be tested by plotting the data in the same manner for two nose Reynolds numbers. The results are given in Fig. 8 for the windward and leeward cone rays. The windward cone data (positive α) do not correlate on this figure. However, far downstream the data at each positive angle of attack separate as a function of nose Reynolds number by approximately the values predicted by the theoretical two-dimensional heat-transfer calculations.[20] [These calculations apply to the cone base for each model configuration ($x/R = 100$, $R = 0.075$ in.; $x/R = 50$, $R = 0.15$ in.)]. It is also observed that the decrease and subsequent increase in the heat-transfer data at $\alpha = 10°$ occurs at different axial locations for the two nose Reynolds numbers as opposed to the pressure

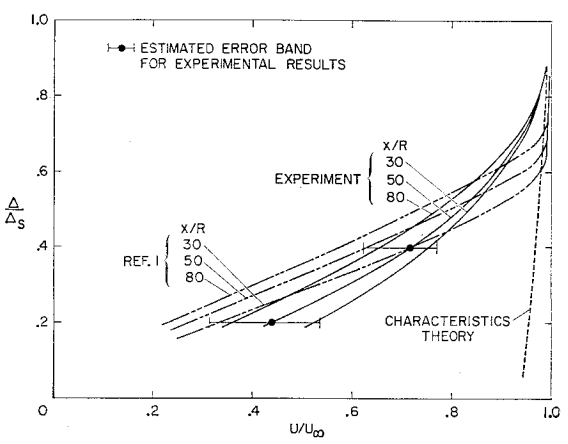

Fig. 6 Velocity profiles through the shock layer; R = 0.075 in., $M_\infty = 40$, $\theta_c = 3°$, $\alpha = 0°$, $T_w/T_o \approx 0.70$, $\gamma = \frac{5}{3}$.

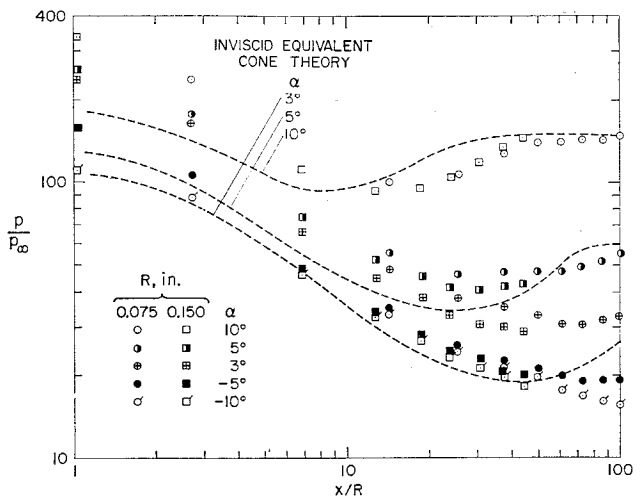

Fig. 7 Pressure distribution on windward and leeward rays at angles of attack; $M_\infty = 40$, $\theta_c = 3°$, $T_w/T_o \approx 0.70$, $\gamma = \frac{5}{3}$.

results for which the location of the overexpansions were independent of nose Reynolds number. Theoretical calculations[21] for cones at angle of attack with negligible cross flow yielded results two to four times greater than the measured heat-transfer data. The present heat-transfer data indicate that boundary-layer flow over the windward cone rays is approaching a two-dimensional character.

Measured shock-wave shapes obtained at $\alpha = 10°$ are presented in Fig. 9 for the windward cone ray. The effect of nose Reynolds number on the shock-wave shape is small. The measurements are compared with the inviscid equivalent cone calculations. The experimental results display a delayed overexpansion compared to the calculations which agrees with the pressure results. Additional data obtained for $T_w/T_o = 0.37$ were similar to those shown in Fig. 9 for $T_w/T_o = 0.70$, with a 2 to 4% reduction in total shock-layer thickness.

Pitot-pressure surveys through the shock layer obtained at various axial stations ($x/R = 10$, 30, and 80) on the windward cone ray at $\alpha = 10°$ are presented in Fig. 10. Also plotted are the results from the inviscid equivalent cone calculations. Over the entire range of x/R there is excellent qualitative agreement between these calculations and the experimental results. Quantitatively, the measured profiles have been compressed toward the shock wave from the inviscid case with a significant boundary layer (up to 40% of the total layer) between the inviscid layer and the body. These results indicate the absence of entropy layer merging with the viscous boundary layer as opposed to the zero angle-of-attack case. Also shown for comparison purposes (Fig. 10c), is a sharp cone pi-

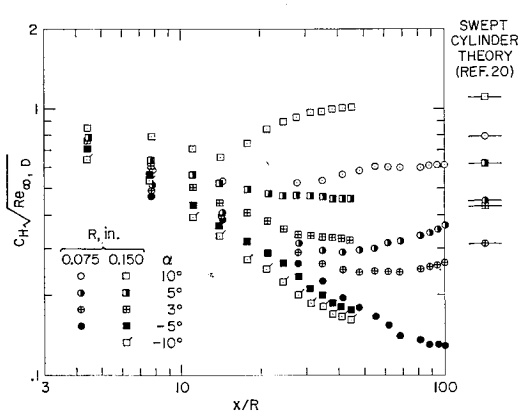

Fig. 8 Heat-transfer distribution on windward and leeward rays at angle of attack; $M_\infty = 40$, $\theta_c = 3°$, $T_w/T_o \approx 0.37$, $\gamma = \frac{5}{3}$.

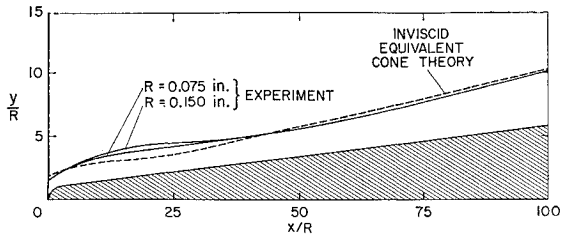

Fig. 9 Shock wave shapes on windward ray; $M_\infty = 40$, $\theta_c = 3°$, $\alpha = 10°$, $T_w/T_o \approx 0.70$, $\gamma = \frac{5}{3}$.

tot-pressure profile obtained for identical flow conditions in Ref. 7. (The small overpressure at $x/R = 80$ could be the result of probe shock-boundary layer interaction.) The data are independent of nose Reynolds number and additional data obtained at $T_w/T_o = 0.37$ indicate exact agreement with the data shown at $T_w/T_o = 0.70$.

IV. Concluding Remarks

The results of the present experimental investigation of blunt slender cones may be summarized as follows:

1) At zero angle of attack, the effect of a large boundary layer on the inviscid flowfield indicated large pressure increases due to viscous-inviscid interaction and significant changes in the inviscid flow-field structure due to boundary-layer entropy-layer coupling. An approximate theoretical inviscid-viscous calculation using a mass balance procedure to determine boundary-layer-edge quantities gave reasonable agreement with the experimentally determined surface quantities and shock-wave shapes. However, for the calculation of the details of a flowfield a more complicated analysis would be required.

2) For a given cone angle, the ratio of local heat transfer to the continuum stagnation point value was found to be independent of Mach and Reynolds number for a wide range of flow conditions including merged layer, strong and weak interaction and thin boundary-layer cone flow regimes.

3) At angle of attack on the windward cone rays the flowfield structure and surface pressure distribution suggest that inviscid equivalent cone techniques are sufficient. However, the surface heat-transfer results indicate that neither equivalent cone nor approximate two-dimensional techniques are sufficient to predict the data.

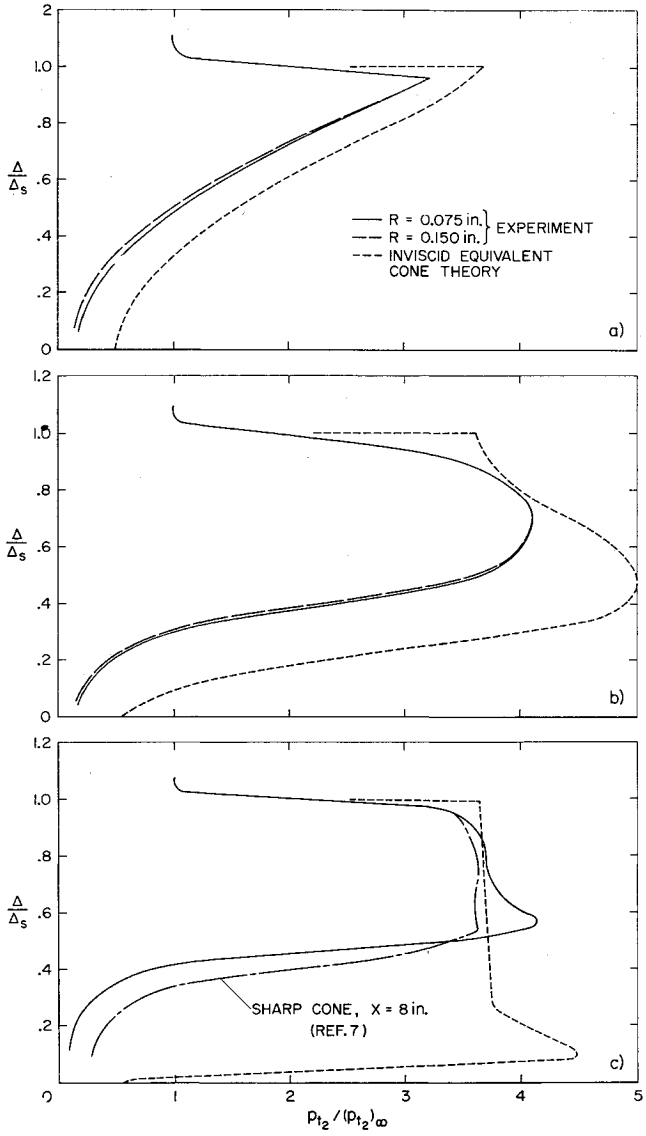

Fig. 10 Pitot-pressure profiles on windward ray; $M_\infty = 40$, $\theta_c = 3°$, $\alpha = 10°$, $T_w/T_o \approx 0.70$, $\gamma = \frac{5}{3}$: a) $x/R = 10$, b) $x/R = 30$, c) $x/R = 80$.

References

[1] Levine, J. N., "Finite Difference Solution of the Laminar Boundary Layer Equations Including Second-Order Effects," AIAA Paper 68-739, Los Angeles, Calif., 1968.

[2] Jackson, S. K., Jr., "The Viscous-Inviscid Hypersonic Flow of a Perfect Gas over Smooth Symmetric Bodies," Ph.D. thesis, 1966, University Microfilms, Ann Arbor, Mich.

[3] Lewis, C. H., "Comparison of a First-Order Treatment of Higher-Order Boundary-Layer Effects With Second-Order Theory and Experimental Data," Ph.D. thesis, 1968, University Microfilms, Ann Arbor, Mich.

[4] Little, H. R. and Marchand, E. O., "Vorticity Influences on Flow Fields of Slender Cones at Hypersonic Speeds," AEDC-TR-68-263, April 1969, Arnold Engineering Development Center, Arnold Air Force Station, Tenn.

[5] Ladyzhenskii, M. D., "Hypersonic Viscous Flow over Slender Bodies," *Priklandnaia Mathematikai Mekhanika*, Vol. 27, No. 5, 1963, pp. 765–778.

[6] Cheng, H. K., "Viscous and Inviscid Slender-Body Problems of Hypersonic Flow," Rept. USCAE 108, Aug. 1969, Univ. of Southern California, pp. 98–101.

[7] Horstman, C. C. and Kussoy, M. I., "Hypersonic Viscous Interaction on Slender Cones," *AIAA Journal*, Vol. 6, No. 12, Dec. 1968, pp. 2364–2371.

[8] Kinslow, M. and Arney, G. D., Jr., "Thermo-Molecular Pressure Effects in Tubes and at Orifices," AGARDograph 119, Aug. 1967.

[9] Conti, R. J., "Approximate Temperature Distributions and Streamwise Heat Conduction Effects in the Transient Aerodynamic Heating of Thin-Skinned Bodies," TN D-895, 1961, NASA.

[10] George, A. R. and Reinecke, W. G., "Conduction in Thin-Skinned Heat Transfer and Recovery Temperature Models," *AIAA Journal*, Vol. 1, No. 8, Aug. 1963, pp. 1956–1958.

[11] McMahon, H. M., "An Experimental Study of the Effect of Mass Injection at the Stagnation Point of a Blunt Body," Memo. 42, May 1958, Graduate Aeronautical Lab., California Institute of Technology.

[12] Horstman, C. C., "Surface Pressures and Shock-Wave Shapes on Sharp Plates and Wedges in Low-Density Hypersonic Flow," *Rarefied Gas Dynamics*, edited by L. Trilling and H. Y. Wachman, Vol. 1, Academic Press, New York, 1969, pp. 593–606.

[13] Inouye, M., Rakich, J. V., and Lomax, H., "A Description of Numerical Methods and Computer Programs for Two-Dimensional and Axisymmetric Supersonic Flow Over Blunt-Nosed and Flared Bodies," TN D-2970, 1962, NASA.

[14] Cheng, H. K., "Hypersonic Flow With Combined Leading-Edge Bluntness and Boundary-Layer Displacement Effect," Rept. AF-1285-A-4, Aug. 1960, Cornell Aeronautical Lab., Buffalo, N. Y.

[15] Lees, L., "Laminar Heat Transfer Over Blunt Nosed Bodies at Hypersonic Speeds," *Jet Propulsion*, Vol. 26, No. 4, April 1956, pp. 259–269.

[16] Mateer, G. G., private communication, Sept. 1969.

[17] Wittliff, C. E. and Wilson, M. R., "Heat Transfer to Slender Cones in Hypersonic Air Flow, Including Effects of Yaw and Nose Bluntness," *Journal of the Aerospace Sciences*, Vol. 29, No. 7, July 1962, pp. 761–774.

[18] Wilkinson, D. B. and Harrington, S. A., "Hypersonic Force, Pressure, and Heat Transfer Investigations of Sharp and Blunt Slender Cones," AEDC-TDR-63-177, Aug. 1963, Arnold Engineering Development Center, Arnold Air Force Station, Tenn.

[19] Van Dyke, M., *Perturbation Methods in Fluid Dynamics*, Academic Press, New York, 1964.

[20] Beckwith, I. E., "Similar Solutions for the Compressible Boundary Layer on a Yawed Cylinder With Transpiration Cooling," TN 4345, 1958, NACA.

[21] DeJarnette, R. F. and Davis, R. M., "A Simplified Method for Calculating Laminar Heat Transfer Over Bodies at an Angle of Attack," TN D-4720, 1968, NASA.

OCTOBER 1970 AIAA JOURNAL VOL. 8, NO. 10

Reaction Product Fluctuations in a Sphere Wake

CARL H. GIBSON,* RUSSELL R. LYON,† AND IAN HIRSCHSOHN†
University of California, San Diego, La Jolla, Calif.

Fluctuations of chemical reaction product were detected in the reacting and nonreacting wake of a sphere. Using the principle of conductometric titration, a single electrode microprobe was used to detect the local concentration of ammonium acetate produced when acetic acid and ammonium hydroxide solutions were injected into the wake of a sphere suspended in the test section of a water tunnel. Reacting and nonreacting wakes were produced when the reactants were injected separately or premixed, respectively. Measurements were taken in the reacting wake with a micro-pH probe in order to have an estimate of the extent of reaction. Data reduction was accomplished using digital techniques. Preliminary results have been obtained that indicate that the distribution of the salt concentration is nongaussian for both reacting and nonreacting wakes. Spectra have been calculated at two wake positions and have similar forms for reacting and non-reacting wakes except at low wavenumber. Inflections from inertial-convective $k^{-5/3}$ subranges to viscous-convective k^{-1} subranges were observed at about $\frac{1}{30}$ of the Kolmogoroff wavenumber.

I. Introduction

UNDERSTANDING the distribution of a product of a chemical reaction in turbulent flow has considerable practical importance in problems such as electromagnetic wave scattering from meteor or missile wakes as well as fundamental importance as a basic unsolved problem of turbulent mixing theory. It is not only unsolved; it is nearly untouched, either theoretically or experimentally.

The simplest nontrivial form of the problem is probably for high Reynolds number flow of constant viscosity and density fluid with infinitely fast (compared to the time of mixing) irreversible reactions of the form $A + B \rightarrow C$. The conservation equations assumed are as follows:

$$d\mathbf{v}/dt = -\text{grad}p/\rho + \nu\Delta\mathbf{v} \quad (1)$$

$$\text{div}\mathbf{v} = 0 \quad (2)$$

$$dC/dt = D\Delta C + S \quad (3)$$

where D is the molecular diffusivity of the product of a chemical reaction C. The problem would be the same as passive scalar mixing of C except for the production term S. For the assumed case of very rapid chemical reaction $S = 0$ except for a vanishingly small volume of fluid representing the reaction surfaces separating regions containing reactants A and B. Consequently, we might expect a number of similarities between the dynamically passive scalar mixing distribution and the reaction product distribution.

The fact that S is not everywhere zero couples Eq. (3) to similar species conservation equations for the reactants A and B, and introduces to the problem additional dimensional parameters describing the reaction order and rate. The assumption of very rapid homogeneous reaction rate permits some simplification of the problem, but it is not clear how S will be distributed, or how its distribution will affect that of C.

Toor[1] has considered the rapid reaction problem and has related the extent of reaction to the degree of mixing in a similar passive scalar mixing system by assuming quantities mixed by turbulence are normally distributed. Keeler's[2] measurements of extent of reaction and mean square passive scalar fluctuations were consistent with Toor's theory although no measurements of the smaller scale distribution of reaction product were predicted or measured. Consequently, two of the goals of the present experiments were to test the assumption that scalar fluctuations mixed by turbulence are gaussian and also to measure the product "fine structure." Because of the localization to reaction surfaces of the production rate, the fine structure is of fundamental importance to the problem.

A further goal of the experiment was the development of techniques for digital data acquisition and computer processing of the turbulent mixing signals. The results of this effort have proved quite encouraging. It is clear that in terms of speed, flexibility, and efficiency, digital techniques open up a new dimension in experimental turbulence research.

Finally, one intention of the measurements was to investigate the spectral form of a scalar mixed by a turbulent wake, not only for comparison with the spectrum of the reacting scalar, but also for its own sake since few such measurements exist for any turbulent flow, and apparently none for sphere wakes.

Presented as Paper 68-686 at AIAA Fluid and Plasma Dynamics Conference, Los Angeles, Calif., June 24–26, 1968; submitted July 24, 1969; revision received January 12, 1970. This research was supported by the Advanced Research Projects Agency of the Department of Defense and was monitored by the U.S. Army Research Office—Durham under Contract DA-31-124-ARO-D-257.

* Assistant Professor, Department of Aerospace and Mechanical Engineering Sciences and Institute for Pure and Applied Physical Sciences.

† Graduate Student, Department of Aerospace and Mechanical Engineering Sciences.